Non-Contact Measurement and Analysis of Trapped Charge Decay Rates for Cable Line Switching Transients

Stephen Robson [1,*] , Abderrahmane Haddad [1] , Simon Dennis [2] and Foroozan Ghassemi [2]

1   School of Engineering, Cardiff University, Cardiff CF24 3AA, UK; haddad@cardiff.ac.uk
2   National Grid, Warwick CV34 6DA, UK; simon.dennis@nationalgrid.com (S.D.);
    forooz.ghassemi@nationalgrid.com (F.G.)
*   Correspondence: robsons1@cardiff.ac.uk; Tel.: +44-29-2087-5351

Abstract: During reclosure of 275 kV cable circuits used for voltage control, excessive overvoltages were observed on the network. Such events cause onerous and costly failures. Transient simulations have shown that the normal voltage on its own cannot generate such excessive switching overvoltages. Initial investigations by the network operator pointed towards trapped charge on the unearthed as the cause of the failures. Measurement of these trapped charge voltages and their slow decay without interfering with the charge has, to the author's knowledge, not been done before in an operational substation. This work introduces a technique to measure trapped charge at a 275 kV substation using the Electrostatic Field Mill. Since the electric field is a proxy measurement of surface voltage, field mills can also be used to measure voltage. In this paper, an on-site substation measurement setup using an electrostatic field mill has been developed for the non-contact measurement of trapped charge voltage on a 275 kV underground cable circuit following switching operations at a National Grid substation. Results of field measurements within the substation and laboratory experimentation are discussed. It is demonstrated that with adequate calibration, achieved by using the known pre-switching power frequency steady state voltage, the slowly decaying DC voltage caused by the cable trapped charge can be measured using this non-contact technique. The correlation between the instantaneous time constant and the relative humidity is also analysed.

Keywords: trapped charge; sheath voltage limiter; SVL; cable; field mill; transient; overvoltage

1. Introduction

When Circuit Breakers (CBs) or isolator switches operate to switch out cables, successive restrikes occur which equalise the potential between the load and de-energised side [1]. This mechanism is responsible for trapped charge accumulation, which without a significant discharge path, may remain on the cable for a period of hours or even days [2]. The decay rate depends on the available leakage paths, including dielectric loss in the cable itself, insulation leakage paths in the bushings of the cable sealing end and leakage through the supporting insulators. The rate of decay may also depend on environmental conditions, such as humidity, though the process in practical systems is still poorly understood.

Should the switching-in operation occur while a proportion of the trapped charge remains on the cable, the transient voltage between phase and ground could be well in excess of 2 p.u. A subsequent closing operation could lead to high overvoltages, placing excessive stress on exposed assets [3]. For example, a trapped charge of 1 p.u indicates that the first breakdown will occur at 2 p.u, with subsequent overvoltages even higher [1]. A particular case which demonstrates the problems this

phenomenon poses will be the focus of this paper. The issue was first investigated after the network operator noted an unusually high rate of Sheath Voltage Limiter (SVL) failure in a 275 kV cable which was routinely exposed to evening and morning switching for voltage control [4]. Detailed simulation studies of the problem revealed that trapped charge magnitudes of just 0.4–0.5 p.u were high enough to moderately stress the SVLs. To confirm the hypothesis that trapped charge was responsible for the SVL failures, empirical measurements of the trapped charge were required.

The network operator required a non-invasive measurement technique to test for the presence of trapped charge. The solution to this challenging constraint was to use a set of three electrostatic Field Mills (FMs) to measure the electric field underneath each of the three horizontally arranged busbars [5,6]. Since these busbars were connected directly to the cable sealing end of the cable under test, the electric field emanating from them is a proxy for trapped charge on the cable. The solution sought by the network operator was required to measure and log the electric field continuously for several hours, within the harsh environment of a 275 kV substation. It was also required that Relative Humidity (RH) and temperature be measured in tandem with the field measurements such that the role of environmental conditions on the rate of decay can be analysed. Such measurements of trapped charge on live networks are rarely reported in the literature. Since it is not possible to directly relate the electric field sensed by the FM to the voltage of the target, a calibration was performed to relate the known steady state AC voltage to the measured field.

This paper begins by providing a review of the previous published work on this project and previous relevant work in the wider literature. The experimental methodology and theoretical considerations are subsequently detailed. The results section presents the experimentally derived data from the 8 separate overnight tests carried out at the 275 kV substation. Finally, the results are discussed. These results are further analysed with emphasis on the change in instantaneous time constant (a sliding window exponential fit) versus RH and time.

2. Background

Previous Work

In [7,8], a simulation model of the West Denmark transmission system is presented for the particular case of modelling cable switching. It is noted that the CB is forced to restrike a half cycle after the switching event, when the voltage difference across its contacts are 2 p.u. Such restrikes are capable of further increasing the overvoltage to 3 p.u or beyond. The study highlights the potential for overvoltages associated with CB operation in the vicinity of underground cables.

In [1], empirical measurements of switch induced transients within a 500 kV substation are presented. It is remarked that the speed of the contact is crucial in the mechanism of charge transfer between successive restrikes. Closing onto a capacitive load is shown to be associated with successive restrikes which follows a staircase pattern. Such behaviour initiates a pattern of steep fronted travelling waves.

It should be noted that experimental methodologies for determining trapped charge have been developed over the years. In [9], a non-destructive method for space charge measurement based on the thermal step method is presented. However, the work is limited to laboratory-based experiments with relatively short cable lengths, in the order of tens of metres.

The substation circuit of interest in this paper was initially investigated in [4]. This work estimated the energy absorption of SVLs due to switching onto trapped charge. It is hypothesised that the observed SVL failure is due to excessive energy absorption as a direct result of daily switching of this nature. A detailed ATP-EMTP study is provided to simulate the local system, showing that (1) With no trapped charge, the SVL energy absorption is below rated levels and (2) With moderate levels of trapped charge, the energy absorption exceeds rated levels. It is recommended that the Capacitive Voltage Transformers (CVTs) are replaced with wound VTs to provide a significant discharge path to trapped charge. This work was further developed in [10], which for the first time, used empirical

measurements of trapped charge. Initial investigations revealed a slowly decaying electric field beneath the cable-connected busbar, strongly indicating the presence of relatively high levels of trapped charge. The present paper extends this work by demonstrating the full set of results over the entirety of the measurement campaign.

The performance of the HVAC cable in switching applications is dealt with comprehensively in [11]. The paper also used a small subset of the experimental data discussed in this paper, alongside laboratory measurements of cable discharge in controlled conditions, to arrive at a simple but accurate model for discharge based on RC circuit theory. A correction factor to account for humidity is proposed.

A key focus of the present paper is to relate the measured decay rate of trapped charge with the atmospheric variables of temperature, Relative Humidity (RH) and Absolute Humidity (AH). Indeed, previous studies have demonstrated that the leakage current in high voltage insulation systems is highly correlated with humidity. In [12], leakage current is measured and correlated with ambient RH for a 25 kV insulation system. A reasonably high correlation is observed (coefficient of determination ≈ 0.6), though the correlation drops in highly polluted insulators. In [13], the leakage current in insulator strings is correlated against temperature and ambient humidity in a 110 kV system. It is observed that the leakage current exhibits a positive correlation with RH (coefficient of determination > 0.8) and a negative correlation with temperature. It is also interesting to note that the monitored leakage current tends to follow a saddle shaped curve, with relatively high levels in the morning and night time, but reaches a minimum in the day time. The tendency for leakage current to correlate with RH is also reported by [14], where a 230 kV AC system is studied. In general, there is broad agreement in the literature that the rate of leakage current increases in the late evening and early morning due to high humidity, relatively low temperatures and associated condensation on the insulator surfaces [15,16]. Such a result may have important implications for the treatment of trapped charge decay rates.

## 3. Experimental Methodology

3.1. Test Conditions

Figure 1a shows a high level diagram of the two substations and cable circuit under test. The section of interest in substation A (S/S A) is made up of a cable sealing end to a 21.74 km underground cable feeder (to S/S B) and a 13.5 m stretch of horizontally arranged busbar to an isolator switch, shown in Figure 1b. The busbar is supported by two sets of insulator poles with a vertical height of 2.4 m. S/S B, which is at the other end of the cable, has a similar setup. Both S/S A and B have capacitive voltage transformers connected to their busbars, so neither have DC discharge capability. The cable connecting S/S A and B uses a crossbonding arrangement to reduce the effects of induced currents. SVLs were used at each minor section.

For voltage control, the network operator switches out the cable (connected to a compensation reactor) every evening. It is subsequently switched back in the morning. Excessive trapped charge left on the cable at the morning switch-in was suspected as the cause of unexpected SVL failure at the minor sections of the cable connecting S/S A and B. This paper reports on a novel experimental procedure which enabled measurement of trapped charge via non-contact DC measurement instruments. The approach chosen was to use a set of three electrostatic FMs placed on an elevated platform underneath each phase of the busbar. Since the busbar remained directly connected to the cable throughout the night, the resulting electric field can be thought of as a proxy for busbar voltage.
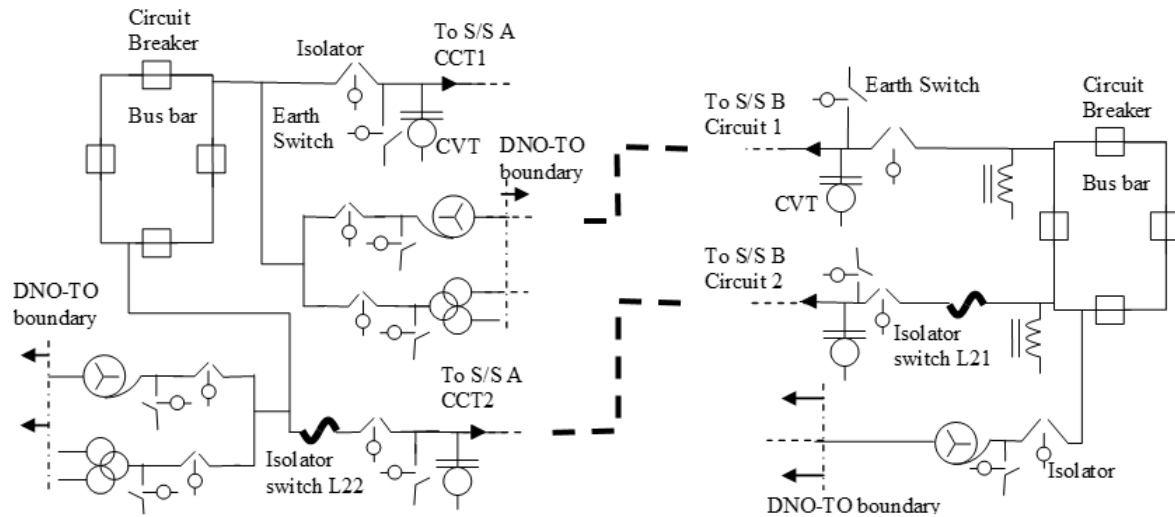
(**a**) Diagram of the two substations connected by the underground cable under test. The experimental setup was set up underneath the busbar on the outgoing circuit 2 from from S/S B.
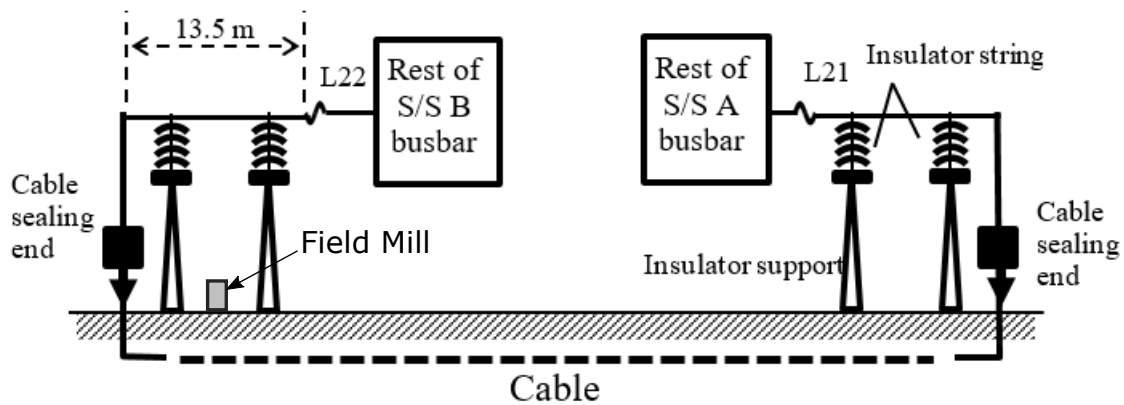
(**b**) Cross section of the test setup. The FMs were positioned underneath the busbar connecting to the cable sealing end.

Figure 1. Diagrams associated with the test setup [10].

3.2. Theoretical Considerations

3.2.1. Electric Field from Busbar Arrangement

The basic test setup involves three electrostatic FMs placed beneath horizontally arranged aerial busbars. The same set of busbars are connected directly to the underground cables via cable sealing ends, as shown in Figure 1b. If the busbars are considered "long", the following gives the potential, V, at a point x m due to a charge density, λ, on a busbar:

$$V(x) = \frac{\lambda}{2\pi\epsilon_0} ln \frac{r_0}{x} \tag{1}$$

where r_0 is the busbar radius and ϵ_0 is the permittivity of free space. Then, since:

$$E(x) = -dV/dx = \frac{\lambda}{2\pi\epsilon_0 x} \tag{2}$$

For a 3 conductor system over a perfectly conducting ground plane, the method of images can be applied, yielding a 6 conductor system. Equation (1) can be converted to matrix form, comprising a 6 by 1 matrix of voltages, [V], a 6 by 6 coefficients of potential matrix, [P], and a 6 by 6 charge matrix, [Q].

$$[V] = \frac{1}{2\pi\epsilon_0}[P][Q] \tag{3}$$

Then, rearranging to obtain the charge matrix:

$$[Q] = \frac{2\pi\epsilon_0}{[P]}[V] \tag{4}$$

The above expressions, with superposition, are used to derive values of electric field magnitude at an arbitrary vertical position of the FM beneath the busbar. The normalised field (normalised to the maximum field obtained at a 4 m height) is shown in Figure 2. The assumption is that a 1 p.u voltage is applied to each busbar, with one of the three at a negative polarity. Based on the restrike charge transfer mechanism outlined in [1], this set of simulations replicates the expected result of one phase exhibiting the reverse polarity of the other two, but with similar magnitudes. Therefore, the busbars are energised to −1/1/1 pu, 1/−1/1 pu and 1/1/−1 pu for red, blue and yellow phases, respectively.
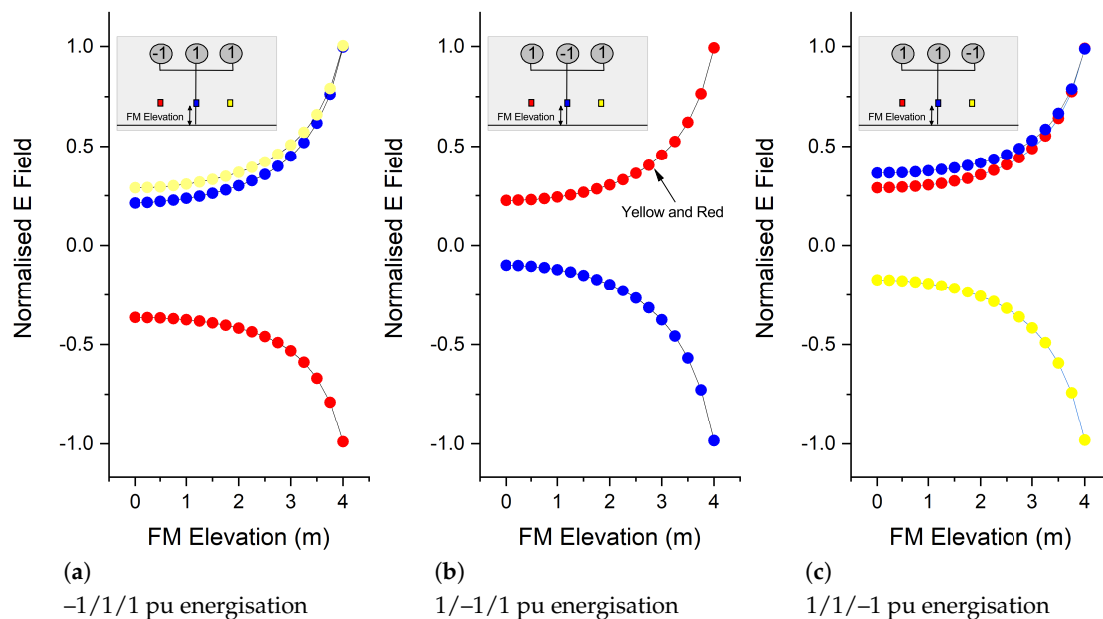

Figure 2. Simulation results showing the normalised electric field magnitude at each FM as a function of elevation for energisation of each busbar of ±1 pu. The polarity of each busbar is signified in the top left of each plot area (note that the diagram is not to scale). The fixed height of the busbars above ground is 4 m and the separation is 6 m.

Figure 2 shows that as the FM moves closer to the busbar, the magnitude of the overall electric field increases. At the same time, the contribution of field from adjacent busbars becomes more tangential. For the three cases shown, the magnitude of the fields at the position of the FMs converges to approximately the same value. At a height of 2.5 m, which is approaching the closest safe distance of the FMs to the busbar, there is an inherent offset between the magnitudes, e.g., a −1/1/1 p.u voltage on the busbars yields a −0.7/0.9/1 field at the FM (normalised to the highest field). These results indicate that the FMs should be placed as close as possible (subject to the relevant safety distances) to (1) provide a greater sensitivity (i.e., FM output voltage per kV on the busbar) and (2) minimise the offset due to fields from adjacent busbars.

3.2.2. Circuit Model of a Discharging Cable

The basic model of a de-energised but charged cable comprises an extremely large shunt resistance and a shunt capacitor, both to ground. The decay curve is then exponential, with a time constant given by [11]:

$$\tau = \frac{1}{RC} \tag{5}$$

Then

$$v(t) = V_m e^{\frac{-t}{\tau}} \tag{6}$$

where V_m is the starting voltage. In practice, the shunt resistance, R, is made up of the parallel combination of the cable leakage resistance, R_{cable}, and an external leakage resistance, R_{ext}, which accounts for the cable sealing ends, bushings and insulator leakage paths for direct current.

$$R_{tot} = \frac{R_{cable} R_{ext}}{R_{cable} + R_{ext}} \tag{7}$$

The type of instrumentation (i.e., voltage and current transformers) used at the substation under test were of the capacitive type, so offered a negligible leakage path at DC.

The capacitance can be found using the geometry and permittivity of the cable:

$$C = \frac{2\pi\epsilon_0\epsilon_r}{ln(r_{out}/r_{in})} \tag{8}$$

The time constant is therefore given by [11]:

$$\tau = \frac{R_{cable} R_{ext}}{R_{cable} + R_{ext}} C = R_{tot} C \tag{9}$$

The time constant is indirectly affected by the humidity due to the fact that outdoor equipment, e.g., cable sealing ends, post insulators and bushings, have a leakage current which was earlier shown to be highly correlated with RH. Therefore, R_{ext} will also be a function of RH. The effect of RH on R_{cable} is far less pronounced [11].

3.3. Design of the Field Mill Site Setup

The FM is screwed by its mounting feet into a vertical orientation above a metallic enclosure. A 7.2 A.h lead acid battery, housed in the enclosure, is used to provide the necessary 12 V supply to the FM with enough capacity for several overnight tests between charges. The enclosure, which is shown in Figure 3, also houses a voltage datalogger capable of logging the ±2 V signal from the FM (±2 V corresponds to the electric field that would be produced by a ± 20 kV or ±200 kV flat surface 30cm from the FM sensing plate, depending on the sensitivity setting) at a sampling rate of 1 sample per second, with memory for up to 7 days of recording. A small hole on top of the enclosure allows for a connection between the FM 8-way DIN connector and the associated 12 V battery supply and datalogger connections within the enclosure. This setup has proven to be reliable over numerous separate overnight tests adding up to several hundred continuous hours of testing over the spring and summer months of 2015. A notable limitation of the setup is the vulnerability of the FM to water damage, meaning tests can only be carried out on nights with a low chance of precipitation in the forecast. A close up of the final assembly is shown in Figure 4.
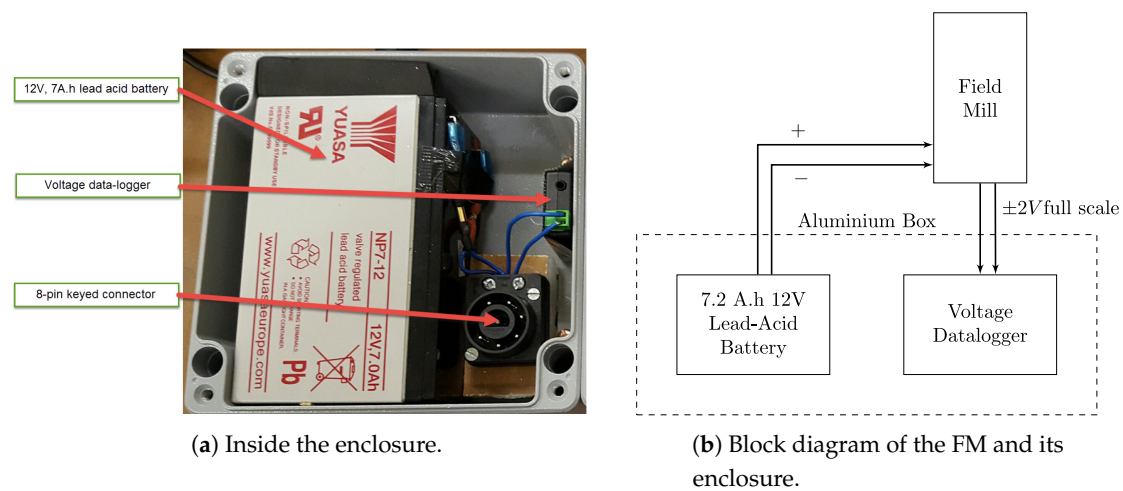
(**a**) Inside the enclosure.

(**b**) Block diagram of the FM and its enclosure.

Figure 3. Experimental apparatus—showing the FM, the enclosure (housing the lead acid battery and temperature/humidity sensor). The FM sits above the box and is connected via a DIN connector through a small hole.

Figure 4. Photograph of the FM inside fabricated enclosure.

3.4. Laboratory Verification

In order to assess the performance of the developed FM test apparatus, preliminary tests were carried at the High Voltage (HV) laboratory. To replicate a relatively slowly decaying voltage source, one of the HV capacitors on a 6-stage marx generator is charged to approximately 20 kV and left to slowly discharge in an open circuit state. The HV terminal of the marx generator is applied to an aluminium bar which is suspended approximately 1m above the FM. An RC voltage divider is used to

step down the HV on the bar. The output of the FM and the divider are connected to an oscilloscope so both can be monitored simultaneously.

Figure 5a shows the plot of FM output voltage and applied voltage as a function of time. It is observed that the FM output closely tracks the actual voltage on the bar, both in the initial charging stage (the voltage rise) and the decay phase (as the voltage drops). Figure 5b shows the correlation of FM output voltage and applied voltage, revealing a generally linear relationship. It is important to note that the relationship between the FM output voltage and the "target" voltage is a complicated function of the surrounding geometry, and the ±20 kV or ±200 kV full range output indication is only relevant to the specific case of the FM sensing a large, flat plate at a distance of 30 cm. An on-site calibration procedure can be used to relate a known voltage to the resultant FM voltage. In this investigation, the known AC steady state voltage is used for calibration purposes.
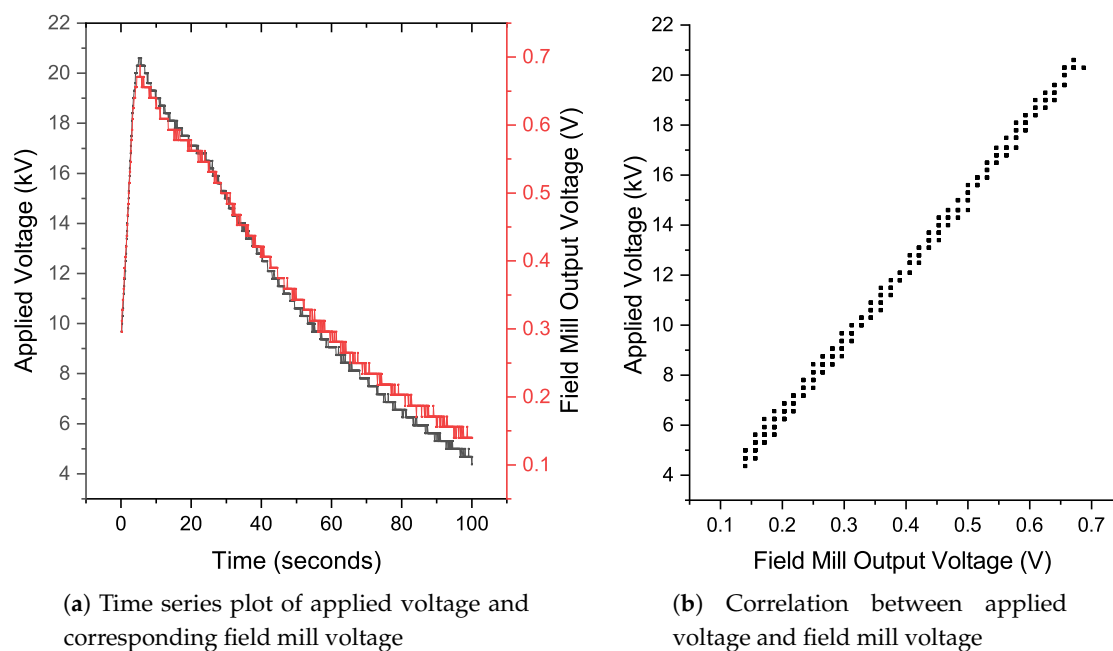

(**a**) Time series plot of applied voltage and corresponding field mill voltage

(**b**) Correlation between applied voltage and field mill voltage

Figure 5. A 4 to 20 kV DC signal is applied to the horizontal bar to simulate the general shape of a decaying exponential. (**a**) shows the time series plot of applied voltage and resulting field mill voltage and (**b**) shows the scatter plot of applied voltage versus field mill voltage.

4. Substation/On Site Results

A photograph of one of the FMs and its associated box is shown in Figure 6. For the first four overnight tests (Figure 7, the FMs were placed close to ground level. For the subsequent four overnight tests, the FM was elevated to a height of approximately 2 m, as depicted in Figure 6. A new calibration factor was calculated to account for the different positions of the FMs. The results obtained during the measurement campaign are shown in Figures 7 and 8. Each graph shows FM voltage, temperature and RH as a function of a common time base, which is derived from the voltage and temperature/humidity/pressure (THP) dataloggers. The sampling rate for the FM voltage and THP dataloggers were 1 sample per second and 1 sample per 30 s, respectively.

Figure 6. Experimental setup showing the arrangement adopted for the FM directly underneath the busbar connected to the charged cable.

For all tests, the FM voltage exhibits a sharp rise in magnitude at a time which corresponds precisely to the evening switching-out of the circuit, as verified by records from the control room. This is followed by a slow, exponential decay. At the time of the morning switching-in event, there remains, in some cases around a third to a quarter of the peak voltage. In other cases, the voltage has decayed to negligible levels. In general, RH appears to be positively correlated with exponential decay rate, especially at values of greater than 80%. This can be observed most prominently in Figure 8c, which shows the recorded values between the 1st and 2nd August. The switching out event occurred at 4 pm, which being a Saturday, is relatively early in comparison to the other tests. At this time, RH was low (around 35%), and steadily increased during the evening until reaching a peak of 100% at approximately 4 am. The decay rate can be visually observed to increase rapidly when the RH exceeds 75%, eventually reaching negligible values some hours before the switching-in event. This test is unusual in that it shows the transition from low (less than 50%) to high relative humidity between switching events. A more detailed analysis of the correlation between RH, AH and exponential decay rate is presented in a later section.

In each test, the magnitudes of the field mill voltages are approximately the same, with one phase exhibiting the reverse polarity compared to the other two. If it is indeed the case that the FM voltages are proportionate to the busbar voltages, this result concurs with observations reported in the literature [1]. The mechanism leading to uniform polarities across all three phases relates to the tendency of an opening switch to successively restrike across the gap, leaving a residual trapped charge on the de-energised side. Therefore, despite each phase switch opening at different times (no point on wave switching was used), the overall mechanism leads to a similar result, albeit with one of the phases always being at the opposite polarity to the other two due to the sequencing of the three phases.
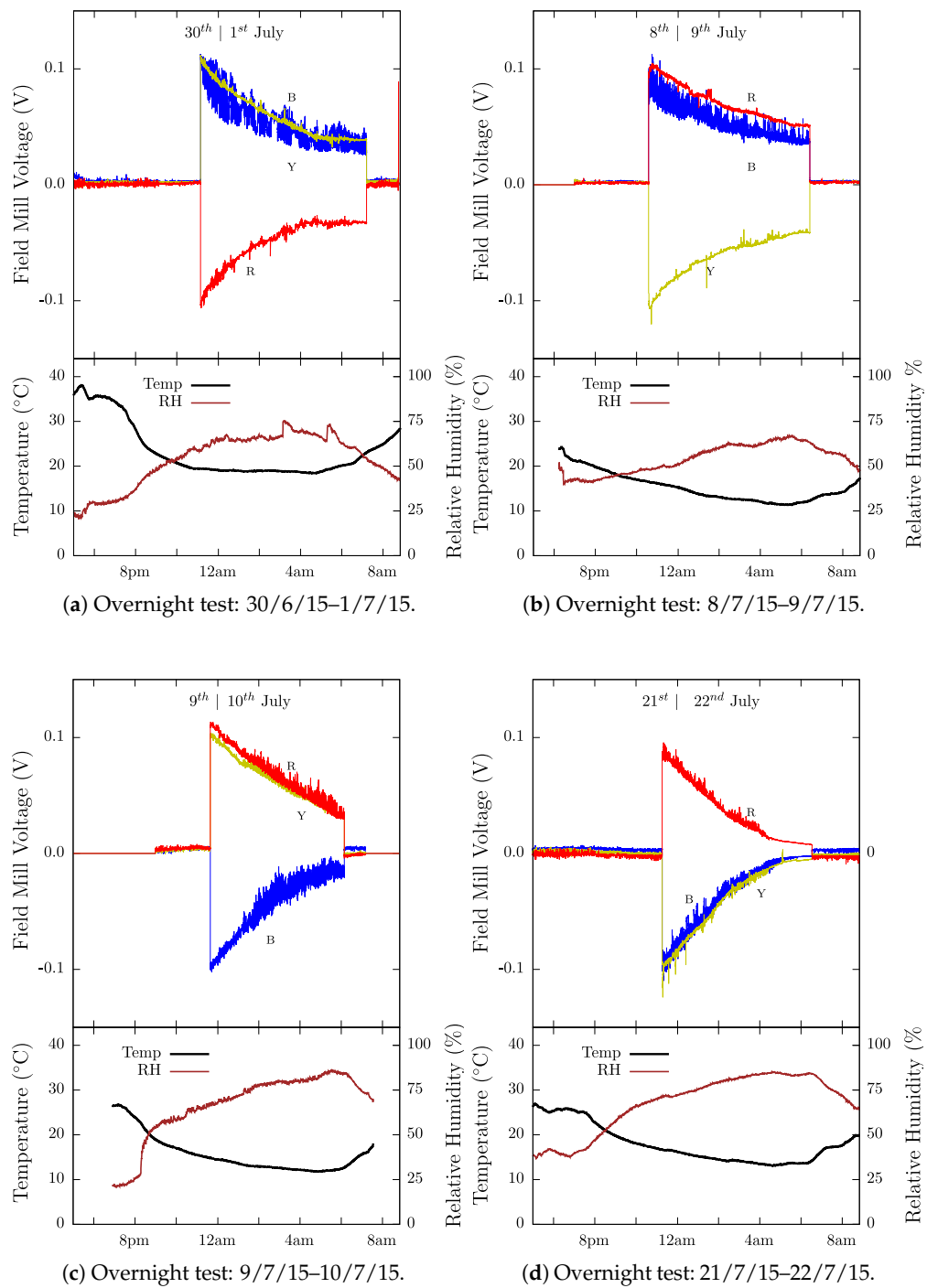
(**a**) Overnight test: 30/6/15–1/7/15.

(**b**) Overnight test: 8/7/15–9/7/15.

(**c**) Overnight test: 9/7/15–10/7/15.

(**d**) Overnight test: 21/7/15–22/7/15.

Figure 7. Recorded Field Mill voltages for each phase (R = Red, Y = Yellow, B = Blue) and RH/temperature plotted on the same time axis.

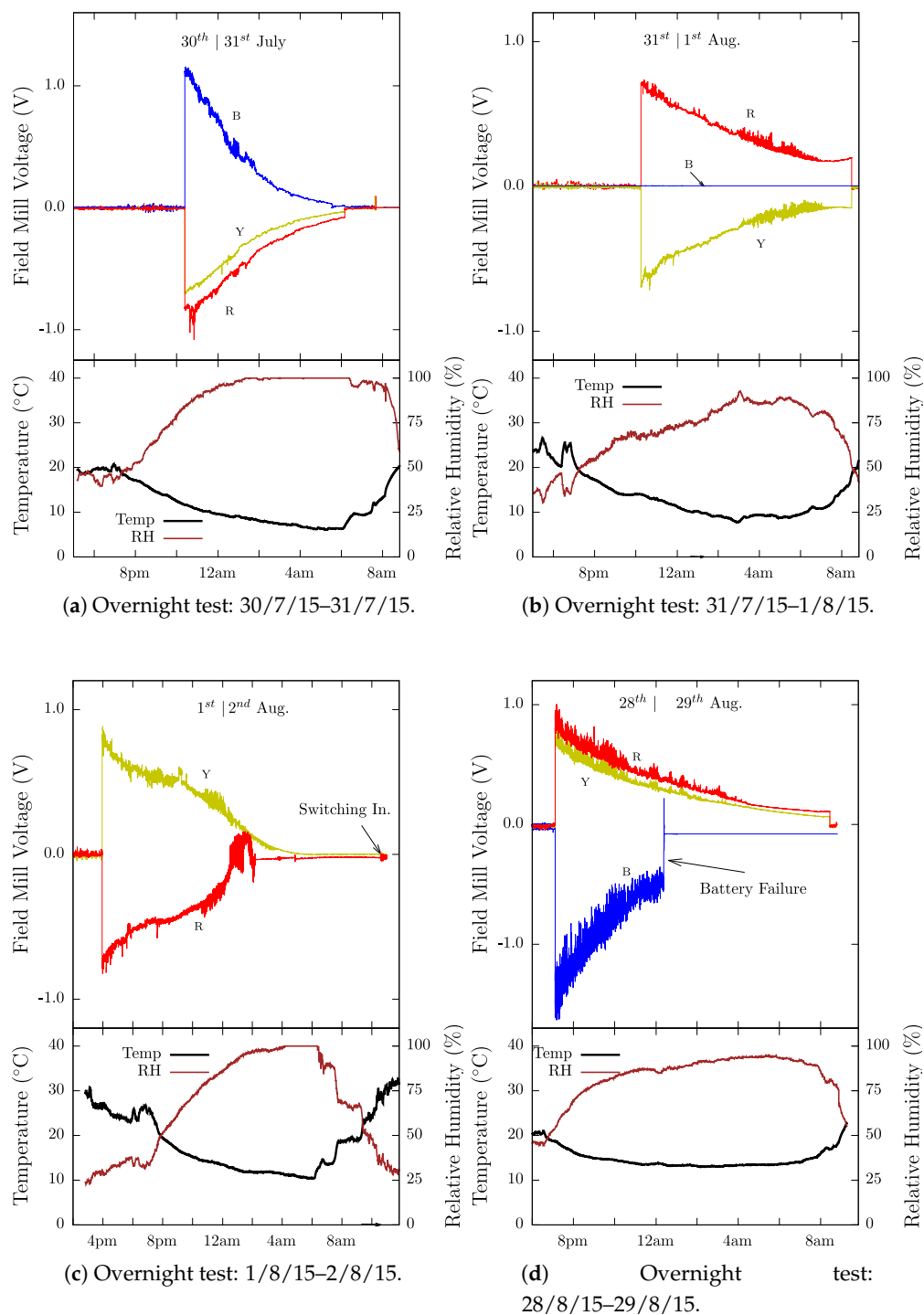**Figure 8.** Recorded Field Mill voltages for each phase (R = Red, Y = Yellow, B = Blue) and RH/temperature plotted on the same time axis.

The sensitivity of the field mill to busbar voltage at its test position can be approximated based on the AC FM voltage underneath the live 275 kV busbar. This calibration procedure was carried out on two occasions, once prior to the test on 14 May 2015 and again prior to the test on the 30 July 2015 due to repositioning of the FM to a greater elevation. Since the FMs were placed directly beneath their respective phases and elevated to a height of approximately 2 metres using platforms, the component of the electric field from adjacent phases was minimised. Furthermore, oscilloscope readings taken during calibration showed precise 120° phase displacements for the entirety of the cycle, indicating

that interference from adjacent phases was small. The calibration data have been used to derive p.u values for each of the tests, as shown in Figure 9. The results show a voltage of between 1 p.u and 4 p.u at the time of switching out, dropping to between 0 p.u and 0.75 p.u at switching in. A study which examined the potential causes of SVL failure rate on the cables considered in this paper concluded that a switching-in magnitude of 0.5 p.u was sufficient to moderately stress the SVLs to their energy rating level [10].
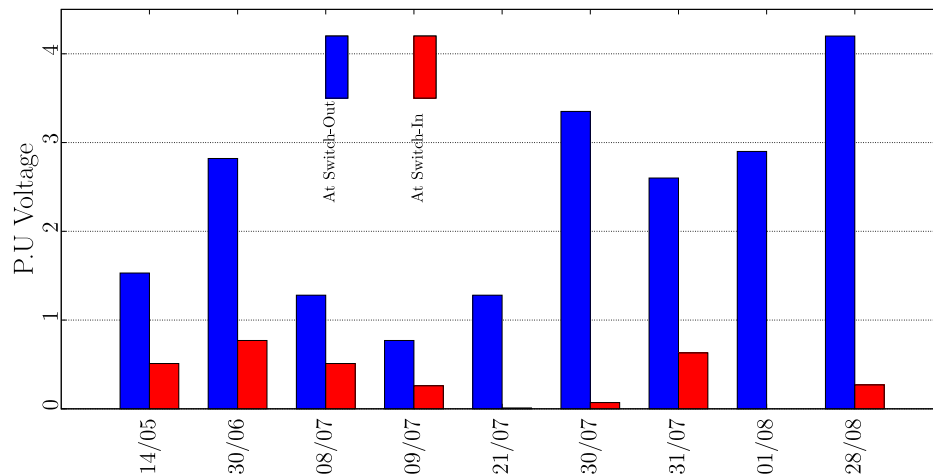
Figure 9. Derived p.u voltages for all tests, calculated using the sensitivity recorded during AC calibration.

5. Analysis of Field Measurement Data

5.1. Adopted Approach for Curve Fitting and Deriving an Instantaneous Time Constant

Due to the observed daily changes in RH and temperature and the known effect this has on the rate of leakage current, an investigation into the changes in "instantaneous" exponential decay rate has been carried out, and will be presented later in this section. However, it is first important to determine whether there is an acceptable fit for the entire discharge curve. The FM voltage data shown in Figures 7 and 8 have been fitted to first order exponentials using the least-squares method. Table 1 shows the results of this analysis, with the RC time constant (τ) and the coefficient of determination (R^2) displayed for each test. In general, the goodness of fit to first order exponential curves is high, with most fits achieving R^2 values greater than 0.9. The outlier, with an R^2 of 0.774, is from the 1st August test. This was the only test to take place on the weekend (Saturday), meaning the scheduled switching-out event was earlier than all other tests. Figure 8a shows that RH started at a lower value (approximately 30%) compared to the other tests, which may explain why the decay curve is a poor fit to a single exponential.

Table 1. Fitting results showing the RC Time Constant and the Coefficient of Determination for each Test.

Test Dates	τ (hours)	R^2
(14/05/15)–(15/05/15)	7.31	0.920
(30/06/15)–(31/06/15)	5.83	0.988
(08/07/15)–(09/07/15)	10.19	0.933
(09/07/15)–(10/07/15)	5.70	0.982
(21/07/15)–(22/07/15)	3.07	0.982
(30/07/15)–(31/07/15)	2.44	0.983
(31/07/15)–(01/08/15)	6.65	0.990
(01/08/15)–(02/08/15)	6.53	0.774
(28/08/15)–(29/08/15)	10.19	0.982

To account for the portion of the RC time constant which varies with atmospheric conditions, an "instantaneous" time constant is calculated on a sample by sample basis. This moving exponential fit allows the time constant to be plotted against the recorded atmospheric conditions, primarily RH and AH.

The procedure is summarised as follows:

1. The raw field mill data is fitted to a high order polynomial function to eliminate noise while preserving the underlying characteristic of the curve.
2. A moving exponential fit, with window size W samples, is performed on the fitted waveform. For an N sample waveform, $N - W$ possible fits exist.
3. The characteristics of the exponential fit, i.e., The RC time constant and R^2 are extracted for each position of the moving window. This is performed on a sample by sample basis, meaning for an N sample signal, $N - W$ possible fits will be produced.
4. The instantaneous time constant, defined as the RC time constant computed for the previous W samples, can be plotted against RH, AH, time etc.

If the time at the instant of switching out (the start of the exponential decay curve) is defined as t_1, and the instant of the switching in (the end of the exponential decay curve) is defined as t_2, the total duration of the curve, rounded to the nearest second, is $N = (t_2 - t_1)$ seconds. This will result in a sample set of $y \in [1, N]$, where y is fitted to an exponential curve using the nonlinear least squares method. The fitting assumes a window size of W samples (or seconds). The window can slide across the data, calculating a new set of parameters for every 1 sample shift. This approach reveals the change in the decay rate over time.

A formalisation of this process is as follows. Assume a first order exponential of the form:

$$y = Ae^{Bx} \tag{10}$$

Nonlinear exponential least squares fitting is defined as:

$$[a_n, b_n] = min \sum_{i=n}^{n+W} y_i \left(\ln y_i - a - bx_i \right)^2 \tag{11}$$

Which produces a set of fitted parameters a_n and b_n, where the latter specifically represents the evolution of the exponential decay curve as a function of time. The coefficient of determination, R^2, is also saved for each fit. The process can be repeated for different window sizes, W, chosen later to be 41, 25 and 17 minutes (arbitrarily chosen). The procedure is carried out in Matlab using the 'exp1' option of the fit function.

Figure 10 shows plots of the raw and polynomial fitted exponential curves, the instantaneous time constant (expressed in hours) and the instantaneous R^2 value, showing the goodness of the exponential fit for the 17, 25, and 41 minute moving windows. In general, the R^2 value remains high for the majority of each test, exceeding 0.99 for each of the 17, 25, and 41 minute window sizes, demonstrating a close fit to the exponential decay curve. There are regions showing drops in the R^2 value which coincide with changes in the instantaneous time constant, B. Towards the end of each test period and just prior to the morning switching event, there is a more pronounced drop in R^2 accompanied by a significant drop in B. This occurs too early to be accounted for by the moving window overlapping the end of the curve (i.e., where it drops to zero). In some cases, for example the tests commencing on the 30th June (Figure 10a), the 8th July (Figure 10b) and the 21st July (Figure 10f), the instantaneous time constant drops considerably at around dawn, coinciding with an increase in temperature and drop in RH. This is a potentially significant observation and as such it will be further analysed later on.
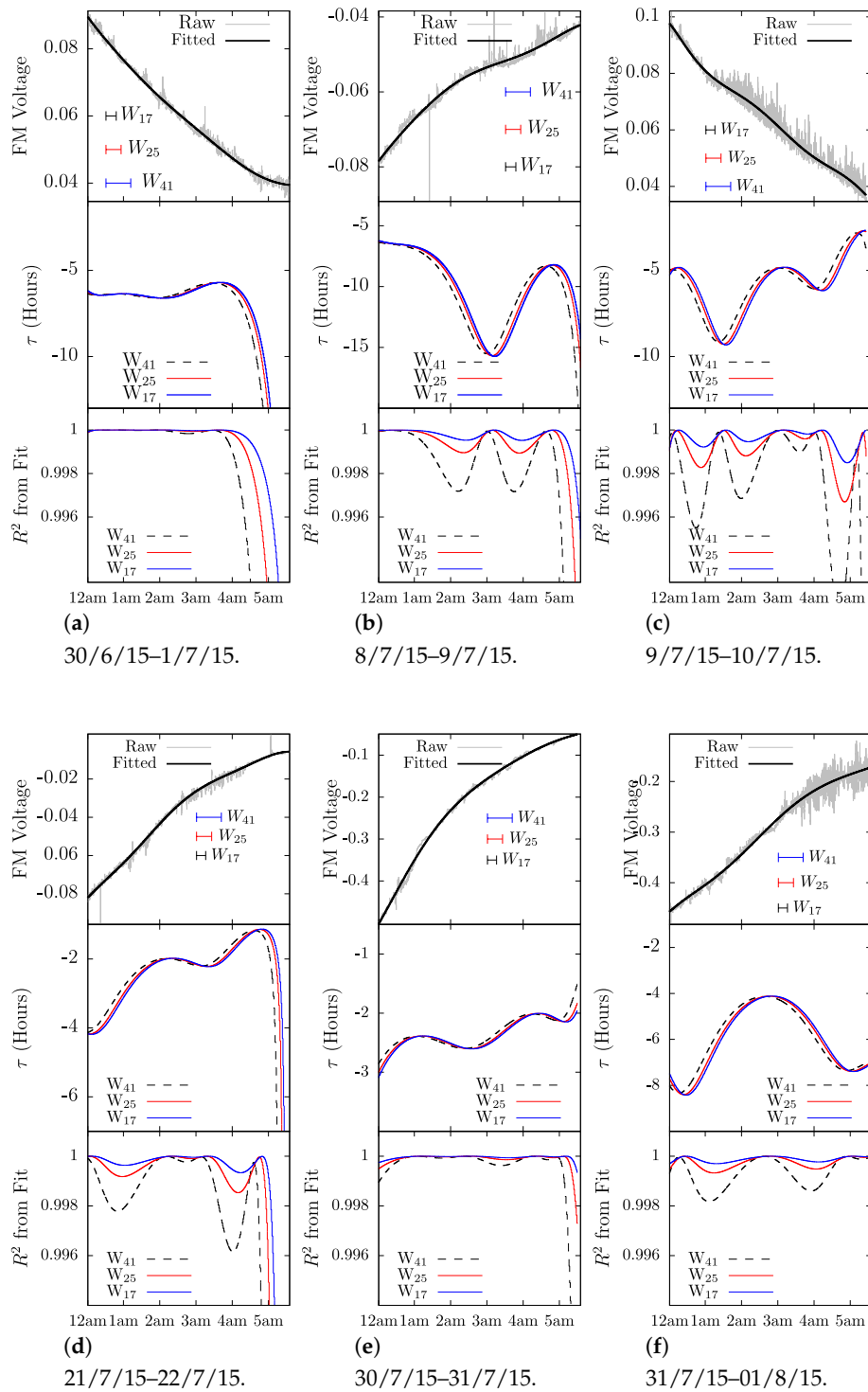
Figure 10. Field Mill Voltage, Instantaneous time constant (τ) and the calculated R^2 from each fit for the three window lengths (41, 24 and 17 min).

5.2. Relationship between Instantaneous Time Constant, RH, AH and Time

Figures 11a,b show scatter plots of instantaneous time constant against RH and AH, respectively—for the entirety of the measurement campaign. The data are color coded to differentiate between different test dates and some data points below τ hours are omitted to preserve clarity. The AH is derived from the recorded RH and temperature according to Equation (12) [17]:

$$AH = \frac{6.112 \cdot exp\left(\frac{17.67 \cdot T}{T+243.5}\right) \cdot RH \cdot 2.1674}{273.15 + T} \quad (12)$$
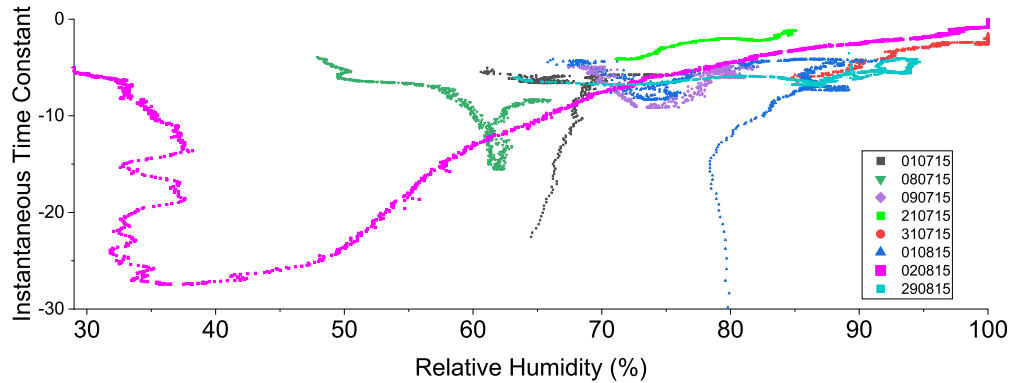
(**a**) Relative Humidity versus instantaneous RC time constant.
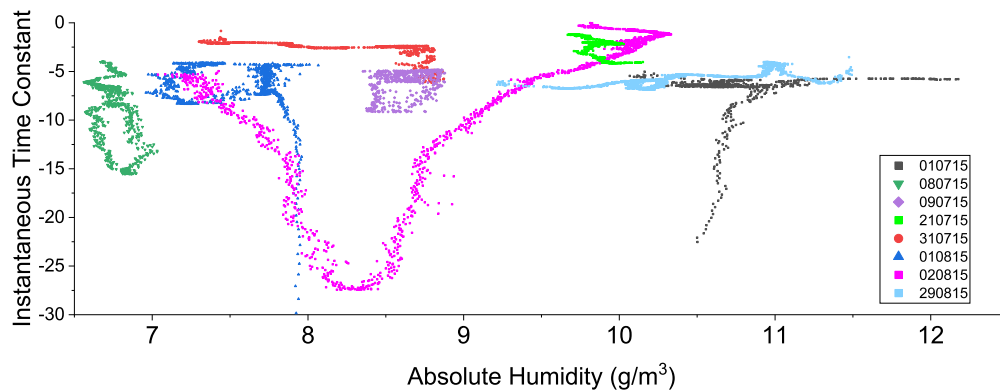
(**b**) Absolute Humidity versus instantaneous RC time constant.

Figure 11. Scatter plots showing AH and RH against the instantaneous RC time constant. The data are colour coded by the date of the observation.

Figure 11a shows a loose positive correlation between RH and τ at relatively low RH (>85%). It is particularly noticeable that some of the dates exhibit a sharp drop off in RH over a quite narrow range of RH. This phenomenon occurs at dawn as the temperature starts to rise. This is noted in Figure 8a, where the switching-in event was scheduled relatively late in the morning. The decay rate of the FM voltage drops significantly at this point. The same phenomenon is evident in Figure 7a and its associated instantaneous τ plotted in Figure 10a. In most other overnight tests, the switching-in event occurred before dawn, so the same behaviour is not observed. The relationship between instantaneous τ and AH is less pronounced, as can be seen in Figure 11b.

Three-dimensional plots of RH, instantaneous time constant (τ) and time are shown for all 8 overnight tests in Figures 12 and 13. The sudden drop off in τ at dawn is now easy to see in the overnight tests of 30/6/15–1/7/15 (Figure 12a) and 31/7/15–1/8/15 (Figure 13b). The same is observed in Figures 12b,d.
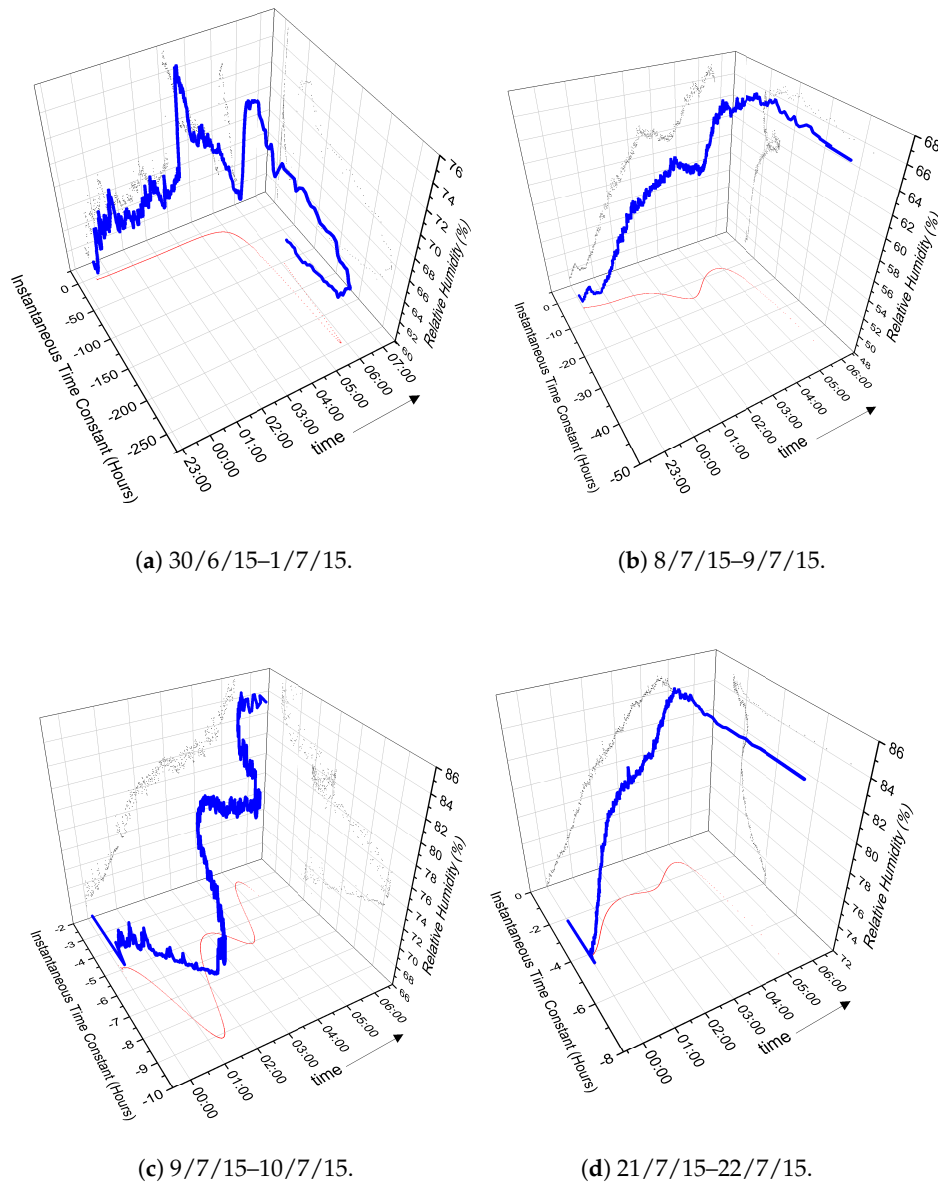
(**a**) 30/6/15–1/7/15.

(**b**) 8/7/15–9/7/15.

(**c**) 9/7/15–10/7/15.

(**d**) 21/7/15–22/7/15.

Figure 12. Relative Humidity plotted against instantaneous time constant and time for the first 4 overnight tests.

Operationally, the difference between discharge rates before and after dawn is an observation worthy of consideration, especially in cases where no obvious path for direct current exists (i.e., where capacitive VTs are used). The observations show that the relative decrease in discharge rate after dawn restricts the effective discharge time to before this point, or before condensation begins to evaporate from the insulator surfaces.

It should also be remarked that in addition to RH, the strength of the wind also plays a role in the distribution of the electric field. This was shown in [18,19], which demonstrates the use of FMs to measure the electric field underneath a HVDC line. This adds a further complication to the process of relating observed FM voltage to actual voltage on the busbar. However, in the cases presented here, the main objective was to reveal the presence of a slowly decaying voltage rather than achieving an accurate estimation of the voltage itself. Future work will attempt to address these issues.
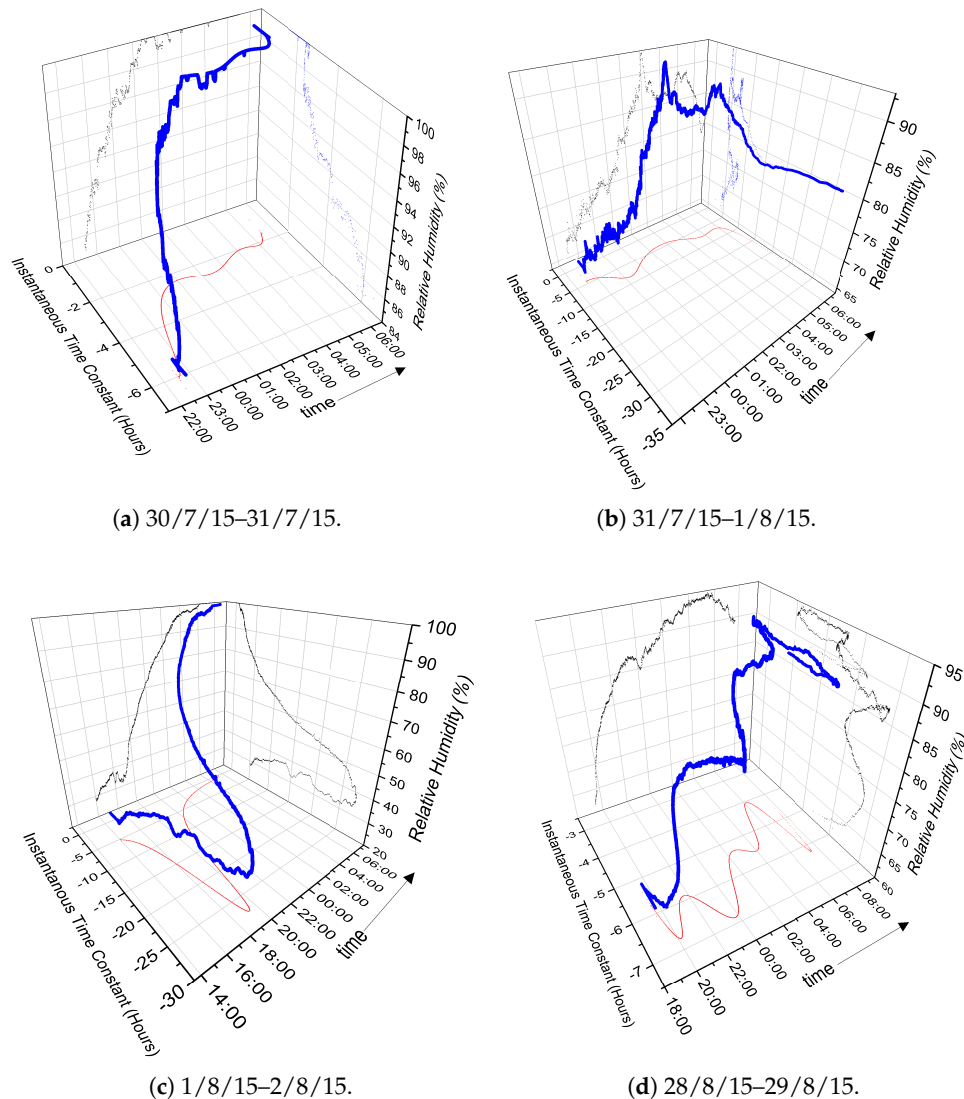
(**a**) 30/7/15–31/7/15.

(**b**) 31/7/15–1/8/15.

(**c**) 1/8/15–2/8/15.

(**d**) 28/8/15–29/8/15.

Figure 13. Relative Humidity plotted against instantaneous time constant and time for the last 4 overnight tests).

6. Conclusions

The tests carried out produced an extensive dataset of RH, AH, temperature, pressure and field mill voltage (a proxy for busbar voltage) on a common time base. The rate of decay is observed to vary widely in the time period between switching events. The association between the instantaneous time constant, which is derived from a moving window exponential fit, and RH, is therefore investigated. It is shown, firstly, that FMs are capable of detecting trapped charge based on the measurement of the electric field, which is considered a proxy of the voltage on the busbar. Second, it is shown that the rate of decay is closely linked to RH, with a higher RH associated with faster rates of decay. In cases where the morning switching in event occurred after dawn, there is an observed sharp decrease in the rate of decay.

References

1. Boggs, S.A.; Chu, F.Y.; Fujimoto, N.; Krenicky, A.; Plessl, A.; Schlicht, D. Disconnect Switch Induced Transients and Trapped Charge in Gas-Insulated Substations. *IEEE Trans. Power Appar. Syst.* **1982**, *PAS-101*, 3593–3602, doi:10.1109/TPAS.1982.317032. [CrossRef]

2. Pordanjani, I.R.; Wang, Y.; Cui, R.; Amiri, E. Discharge characteristics of trapped charge in power lines with underground cable and overhead line segments. In Proceedings of the 2016 IEEE/IAS 52nd Industrial and Commercial Power Systems Technical Conference (I CPS), Detroit, MI, USA, 1–5 May 2016; pp. 1–6, doi:10.1109/ICPS.2016.7490229. [CrossRef]

3. Das, J. *Transients in Electrical Systems: Analysis, Recognition, and Mitigation*; McGraw-Hill Professional: New York, NY, USA, 2010; doi:10.1036/9780071626033. [CrossRef]

4. Ghassemi, F. Effect of trapped charges on cable SVL failure. *Electr. Power Syst. Res.* **2014**, *115*, 18–25, doi:10.1016/j.epsr.2014.03.020. [CrossRef]

5. Secker, P. The design of simple instruments for measurement of charge on insulating surfaces. *J. Electrostat.* **1975**, *1*, 27–36, doi:10.1016/0304-3886(75)90005-4. [CrossRef]

6. Chubb, J.N. Two new designs of 'field mill' type fieldmeters not requiring earthing of rotating chopper. *IEEE Trans. Ind. Appl.* **1990**, *26*, 1178–1181, doi:10.1109/28.62405. [CrossRef]

7. Da Silva, F.F.; Bak, C.L.; Holst, P.B. Estimation of the Required Modeling Depth for the Simulation of Cable Switching in a Cable-Based Network. *IEEE Trans. Power Deliv.* **2012**, *27*, 1902–1908, doi:10.1109/TPWRD.2012.2187684. [CrossRef]

8. Da Silva, F.F.; Bak, C.L.; Holst, P.B. Switching Restrikes in HVAC Cable Lines and Hybrid HVAC Cable/OHL Lines. In Proceedings of the 2011 International Conference on Power System Transients (IPST), Delft, The Netherlands, 14–17 June 2011.

9. Castellon, J.; Notingher, P.; Agnel, S.; Toureille, A.; Brame, F.; Mirebeau, P.; Matallana, J. Electric field and space charge measurements in thick power cable isulation. *IEEE Electr. Insul. Mag.* **2009**, *25*, 30–42, doi:10.1109/MEI.2009.4977240. [CrossRef]

10. Ghassemi, F.; Dennis, S.; Ainsley, A.; Haddad, A.M.; Robson, S. 275 kV cable discharge field measurement and analysis of SVLs chain failure using ATP. *Electr. Power Syst. Res.* **2018**, *161*, 95–102, doi:10.1016/j.epsr.2018.04.009. [CrossRef]

11. Lafaia, I.; Ghassemi, F.; Ametani, A.; Mahseredjian, J.; Dennis, S.; Haddad, A.M.; Robson, S. Experimental and Theoretical Analysis of Cable Discharge. *IEEE Trans. Power Deliv.* **2017**, *32*, 2022–2030, doi:10.1109/TPWRD.2016.2602361. [CrossRef]

12. Meyer, L.H.; Oliboni, C.R.P.; Graziano, G.C.; Mustafa, T.I.A.H.; Almaguer, H.A.D.; Molina, F.H.; Cassel, G. A study of the correlation of leakage current, humidity and temperature of 25 kV insulators in urban and rural areas. In Proceedings of the 2011 Annual Report Conference on Electrical Insulation and Dielectric Phenomena, Cancun, Mexico, 16–19 October 2011; pp. 398–402, doi:10.1109/CEIDP.2011.6232679. [CrossRef]

13. Wang, J.; Xi, Y.; Fang, C.; Cai, L.; Wang, J.; Fan, Y. Leakage Current Response Mechanism of Insulator String With Ambient Humidity on Days Without Rain. *IEEE Access* **2019**, *7*, 55229–55236, doi:10.1109/ACCESS.2019.2910660. [CrossRef]

14. Fontana, E.; Oliveira, S.C.; Cavalcanti, F.J.M.M.; Lima, R.B.; Martins-Filho, J.F.; Meneses-Pacheco, E. Novel sensor system for leakage current detection on insulator strings of overhead transmission lines. *IEEE Trans. Power Deliv.* **2006**, *21*, 2064–2070, doi:10.1109/TPWRD.2006.877099. [CrossRef]

15. Suwarno, S.; Parhusip, J. Effects of Humidity and Fog Conductivity on the Leakage Current Waveforms of Ceramics for Outdoor Insulators. *WSEAS Trans. Syst.* **2010**, *9*, 442–452.

16. Werneck, M.M.; dos Santos, D.M.; de Carvalho, C.C.; de Nazaré, F.V.B.; da Silva Barros Allil, R.C. Detection and Monitoring of Leakage Currents in Power Transmission Insulators. *IEEE Sens. J.* **2015**, *15*, 1338–1346, doi:10.1109/JSEN.2014.2361788. [CrossRef]

17. WMO. *Guide to Instruments and Methods of Observation*; World Meteorological Organization: Geneva, Switzerland, 2008.

18. Zhen, Y.; Cui, X.; Lu, T.; Wang, X.; Wang, D.; Liu, Y.; Ma, W.; Xiang, Y. A Laboratory Study on the Ion-Flow Field Model of the DC Wires in Stable Wind. *IEEE Trans. Power Deliv.* **2015**, *30*, 2346–2352, doi:10.1109/TPWRD.2015.2444372. [CrossRef]

19. Cui, Y.; Yuan, H.; Song, X.; Zhao, L.; Liu, Y.; Lin, L. Model, Design, and Testing of Field Mill Sensors for Measuring Electric Fields Under High-Voltage Direct-Current Power Lines. *IEEE Trans. Ind. Electron.* **2018**, *65*, 608–615, doi:10.1109/TIE.2017.2719618. [CrossRef]